IEEJ Journal of Industry Applications
Vol.6 No.3 pp.213–222 DOI: 10.1541/ieejjia.6.213

Paper

Lamb-Wave Resonator Oscillator Powered by Inductive Compensation of Stray-Capacitance CMOS Inverter

Tomio Sato* Non-member, Masahide Marumo** Non-member
Tetsuya Akitsu*a) Member

(Manuscript received June 29, 2016, revised Nov. 15, 2016)

In this study, we studied Lamb wave resonator driver circuit with inductive compensation of the internal capacitance to improve the frequency limit by the transition frequency f_T which is one of the important parameters of active components for deciding amplification and oscillation. Comparing with an SAW resonator, the Lamb-wave oscillator can provide highly stable frequency-temperature characteristics and smaller frequency deviation at the normal temperature. The inductive cancellation scheme of the internal capacitor of the CMOS inverter realizes oscillation over f_T.

Keywords: f_T, SAW, Lamb-wave oscillator

1. Introduction

Recently communication networks are increasing in speed and volume and network traffic keeps increasing. A high-frequency, low power, stable clock is needed in telecommunication infrastructure. In a recent work on the high frequency fundamental (HFF) oscillator, the active component was selected among discrete bipolar devices: a germanium silicon transistor [(1)]. In the industrial solution for high-performance, a significant part of the production is realized by a mixed digital-analogue complementary metal oxide semiconductor field effect transistor (CMOS FET) technology enforced as an integrated digital and analog circuit [(2)]. One of the engineering issues for quartz crystal oscillators is oscillation at higher frequencies. Several works report the modification of the conventional Pierce oscillator circuit for higher-frequency oscillation. This circuit has lower negative resistance in the high frequency region. A popular scheme to expand the oscillation region is the use of an inductor connected to the quartz resonator in series. This circuit shows transition between quartz resonance and LC resonance oscillation and the inherent short-comings for high frequency oscillation. In this work, we develop a compensation scheme of the internal capacitance using an inductor connected between the input and output terminal of the active circuit. Engineering issues are suppression of the LC oscillation and extension of the operational frequency limit of the CMOS-inverter. The compensation of input capacitance of the CMOS inverter with an inductor is operable at frequencies higher than the nominal transition frequency of the CMOS inverter. The Lamb-wave resonator has been studied by Nakagawa et al., at the University of Yamanashi, as a future candidate for a high frequency oscillator using the piezoelectric resonators [(3)–(8)]. In general cases, high frequency time base can be realized by the fundamental resonance oscillation with a SAW resonator, which provides better performance of jitter characteristics of the signal compared with the phase-locked-loop (PLL) frequency multiplication technique using AT-cut quartz resonance oscillation. Lamb waves combine both primary longitudinal waves (P waves) and shear vertical/transverse waves (SV waves), which change modes and converge at the upper and lower boundaries. As Lamb waves propagate through a piezoelectric material, a compound mode is formed of four waves with additional electromagnetic waves. Confined to a depth of roughly one wavelength from the surface, surface acoustic waves propagate mainly along the x-axis at a slow rate. In contrast, with the Lamb wave, the entire plate vibrates. Depending on how the longitudinal and transverse waves converge, various modes can emerge, ranging from the slow-rate mode to the fast-rate mode. The developed Lamb-wave resonator is comparable with standard SAW resonators with respect to the jitter characteristics, or phase noise. Providing the same performance in the high-frequency region, better frequency deviation characteristics at normal temperature and frequency-temperature characteristics can be realized. In spite of the complicated nature, the Lamb-wave resonator can be simplified to the same model as an ordinary quartz crystal resonator. The resonance oscillation of the Lamb-wave resonator oscillator is demonstrated at 442 MHz using a low-cost CMOS single gate inverter. The Lamb resonator oscillator shows the level of the phase noise comparable with a SAW resonator and higher stability with respect to variation of the ambient temperature.

a) Correspondence to: Tetsuya Akitsu. E-mail: akitsu@yamanashi.ac.jp
* Human Science, Environmental and Medical Engineering Division, Integrated Graduate School of Medicine, Engineering and Agricultural Science, University of Yamanashi
4-3-11, Takeda, Kofu, Yamanashi 400-8511, Japan
** River Eletec Corporation
2-1-11, Fujimi-ga-oka, Nirasaki, Yamanashi 400-8502, Japan

2. Circuit Design and Analysis

2.1 Analysis of the Quartz Resonance Oscillator

Figure 1 shows the circuit diagram. Complex impedances

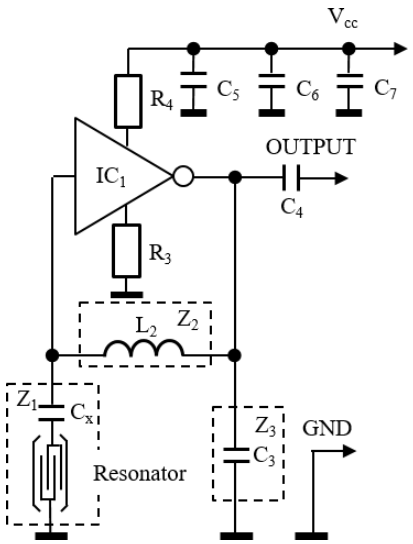

Fig. 1. High frequency LAMB-wave resonator oscillator

represent axial inductor L_2, ceramic capacitor C_3 and a Lamb-wave resonator. At the high-frequency region, inductance L_p is treated with resistance r_p, and internal capacitance c_p. C_x is a capacitor for tuning. C_3 is a capacitor for the local-resonator. C_4 is coupling capacitor. C_5, C_6, and C_7 are distributed pass-capacitors connecting between V_{cc} and ground lines. R_3 and R_4 are feedback resistors for the gain control and the protection against the surge. The transconductance is aimed at the branch to be led to the resonance oscillation, because LC oscillation is excited in the case that g_m is excessively large. We will discuss this in detail later.

Table 1 shows circuit constants in the analysis and experiment. Tables 2 and 3 show the equivalent circuit components of the Lamb-wave resonator and a SAW resonator as a standard. Central part of a quartz substrate was processed by the photolithography to a reduced constant thickness and IDT launching electrode for Lamb wave and two IDT reflectors were placed on the flat surface. The oscillation frequency $F_r = 441.951$ MHz concurs with the theoretical estimation of the Lamb-wave resonance.

These resonators are prototypes produced for the present research purpose, and there is no catalogue number attributed.

IC_1 is a non-buffer type CMOS inverter, which is selected from low-cost unbuffered CMOS inverter TC-7SUG04F. Figure 2 shows simplified oscillator circuit: equivalent circuit-1.

The frequency limit is determined by internal capacitors. $C_{p:gd}$ and $C_{p:gs}$ for P-channel MOSFETS, $C_{n:gd}$ and $C_{n:gs}$ for N-channel MOSFETs are gate-drain and gate-source capacitances, respectively.

$$\begin{aligned} C_{p:gs} &= C_{n:gs} = C_{gs}, \\ C_{p:gd} &= C_{n:gd} = C_{gd}. \end{aligned} \quad \cdots\cdots (1)$$

$$\begin{aligned} C_{3o} &= C_3 + C_{os}, \\ C_{di} &= 2C_{gd} + c_{io}. \end{aligned} \quad \cdots\cdots (2)$$

c_{os} and c_{io} are drain-ground and drain-gate capacitance. C_{di} is composed capacitance of C_{gd} and c_{io}. C_{3o} is composed capacitance of C_3 and c_{os}. Capacitances are set equal.

L_p, r_p, and c_p are composed to equivalent resistance r_q.

Table 1. Circuit constants

Symbol	Unit	Value	Reference
L_2	nH	47	r_p=1.44 Ω, C_p= 0.37 pF
C_3	pF	open	C_5 = 0.1 μF, C_6 = 10 μF
C_4	pF	1	Output coupling capacitor
C_x	pF	1000	Adjustment capacitor, variable.
c_{io}	pF	0.1	Capacitance between the input and output.
c_{io}	pF	2.8	Capacitance between the output and ground.
$C_{p:gs}$, $C_{n:gs}$	pF	1.5	Gate-source capacitance
$C_{p:gd}$, $C_{n:gd}$	pF	0.01	Gate-drain capacitance
V_{cc}	V	2.5	
C_z	pF	2	Replaced capacitor for C_0 in the LC oscillator mode

IC_1: CMOS inverter TC-7SUG04F

Table 2. Equivalent circuit constant

C_0 (pF)	C_1 (fF)	L_1 (μH)	R_1 (Ω)	F_1 (MHz)
4.1	3	43.2	22.95	442.097

LAMB-wave resonator: F_r = 441.951 MHz (Typical value).

Table 3. Equivalent circuit constant

C_0 (pF)	C_1 (fF)	L_1 (mH)	R_1 (Ω)	F_1 (MHz)
3.3	2.3	56	20.1	443.468

SAW-resonator: F_r = 443.905 MHz (Typical value).

Then, r_q and inductance L_q are found.

$$\begin{aligned} r_q &= \frac{r_p}{\left\{1-\left(\frac{\omega}{\omega_p}\right)^2\right\}^2 + \left(\frac{\omega}{\omega_q}\right)^2}, \\ L_q &= L_p \frac{1-\left(\frac{\omega}{\omega_p}\right)^2 - \left(\frac{\omega_p}{\omega_q}\right)^2}{\left\{1-\left(\frac{\omega}{\omega_p}\right)^2\right\}^2 + \left(\frac{\omega}{\omega_q}\right)^2}. \end{aligned} \quad \cdots\cdots (3)$$

Frequencies are defined as in the following forms.

$$\omega_p^2 = \frac{1}{L_p c_p}, \quad \omega_q = \frac{1}{c_p r_p}. \quad \cdots\cdots (4)$$

IC_1 is represented with a part of the MOSFETs, and each active component is replaced with constant current source, $g_m V_{gs}$, where the equal intensity of V_{gs} is applied between the gate and the source. Figure 3 shows equivalent circuit-2.

The direction of current flow is indicated. C_{gs} is the capacitance between the gate and the source. V_{gs} and I_f are found. V_{in} is the gate voltage with respect to the ground level and I_{in} is input current. The feedback resistors are set to $R_3 = R_4 = R_f$.

$$V_{gs} = Z_s I_s \quad \cdots\cdots (5)$$

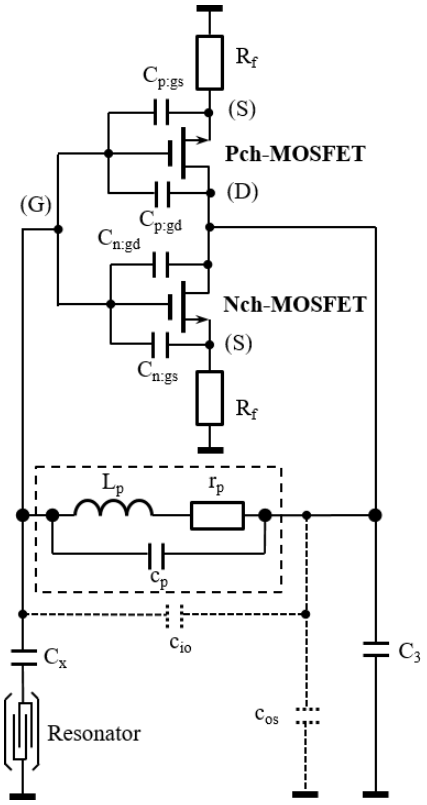

Fig. 2. Simplified oscillator circuit. Equivalent circuit-1

$$I_f = (1 + g_m Z_s) I_s \quad \cdots\cdots (6)$$

where $g_m = g_{mp} - g_{np}$.

$$V_{in} = Z_s I_s + R_f I_f = Z_s I_s + R_f (1 + g_m Z_s) I_s \quad \cdots\cdots (7)$$

$$I_{in} = 2 I_s \quad \cdots\cdots (8)$$

Input impedance is defined.

$$Z_{in} = \frac{V_{in}}{I_{in}} = R_{in} + \frac{1}{j\omega C_{in}} = \frac{R_f + (1 + g_m R_f) Z_s}{2} \quad \cdots\cdots (9)$$

where,

$$Z_S = \frac{1}{j\omega C_{gs}}$$

The real part of the input impedance is R_{in}, and the input impedance is expressed in the terms of the reciprocal of equivalent capacitance C_{in}.

$$R_{in} = \frac{R_f}{2}, \quad \frac{1}{C_{in}} = \frac{1 + g_m R_f}{2 C_{gs}} \quad \cdots\cdots (10)$$

Output current I_{out} is expressed in the following form. Now, C_{gs} and R_{f} are included in transconductance G_{M}. Admittance G_{m} and the imaginary part capacitance C_{m} are found.

$$I_{out} = 2 g_m V_{gs} = 2 g_m Z_S I_S \quad \cdots\cdots (11)$$

$$G_M = \frac{I_{out}}{V_{in}} = G_m + j\omega C_m \quad \cdots\cdots (12)$$

Here G_M is the total response of the circuit, and G_m is the admittance including the current feedback. The small character g_m is the transconductance determined by the gate.

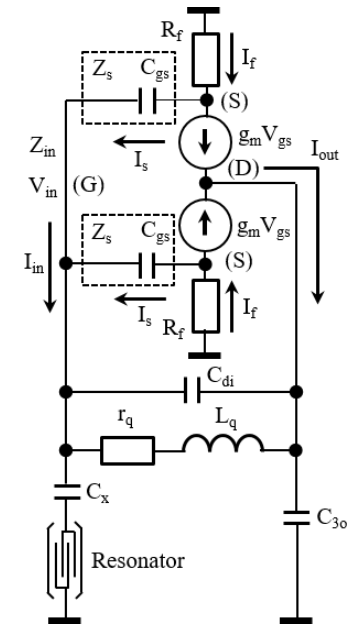

(a) Equivalent circuit-2

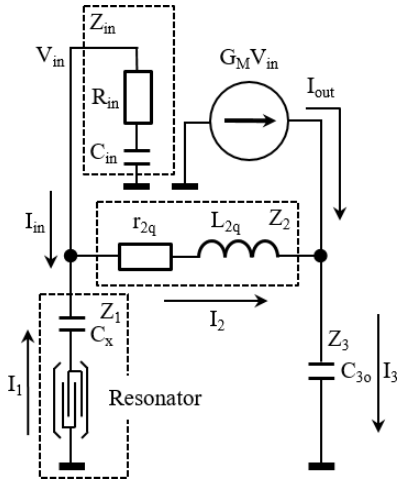

(b) Equivalent circuit-3

Fig. 3. Equivalent circuit with input capacitance C_{gs}

$$G_m = 2 g_m \frac{1 + g_m R_f}{(1 + g_m R_f)^2 + (\omega C_{gs} R_f)^2},$$
$$C_m = -2 g_m \frac{C_{gs} R_f}{(1 + g_m R_f)^2 + (\omega C_{gs} R_f)^2}. \quad \cdots\cdots (13)$$

C_{di}, r_{q}, and L_{q} are parallel composed in the further calculation and setting frequencies in the following forms, resistance $r_{2\mathrm{q}}$ and inductance $L_{2\mathrm{q}}$ are found.

$$r_{2q} = \frac{r_q}{\left(1 - \frac{\omega^2}{\omega_{2p}^2}\right)^2 + \left(\frac{\omega}{\omega_{2q}}\right)^2},$$
$$L_{2q} = \frac{L_p \left(1 - \frac{\omega^2}{\omega_{2p}^2} - \frac{\omega_q^2}{\omega_{2q}^2}\right)}{\left(1 - \frac{\omega^2}{\omega_{2p}^2}\right)^2 + \left(\frac{\omega}{\omega_{2q}}\right)^2}. \quad \cdots\cdots (14)$$

Frequencies are defined as in the following forms.

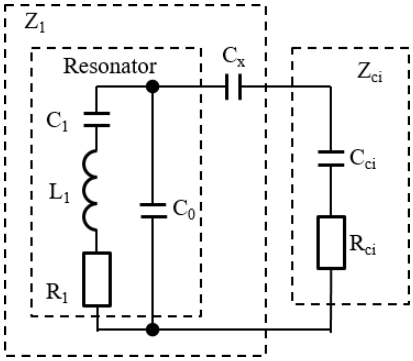

(a) Equivalent circuit-4

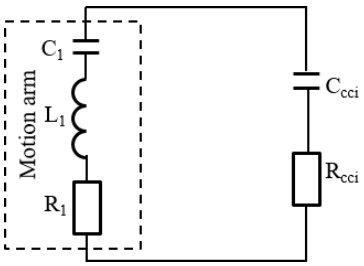

(b) Equivalent circuit-5

Fig. 4. Simplified oscillator circuit

$$\omega_{2p}^2 = \frac{1}{C_{di}L_q}, \quad \omega_{2q} = \frac{1}{C_{di}r_q}. \cdots\cdots (15)$$

Now, $V_{\rm in}$ and $I_{\rm out}$ are expressed in terms of $I_{\rm in}$.

$$V_{in} = Z_{in}I_{in} \cdots\cdots (16)$$
$$I_{out} = G_M V_{in} = G_M Z_{in} I_{in}. \cdots\cdots (17)$$

Here, equivalent circuit-3 is found. Applying Kirchhoff's law, homogeneous system (18) is found. Then, the condition for the non-zero solution of the current vector, normal equation is found.

$$\begin{bmatrix} 1 & -1 & 0 & 1 \\ 0 & 1 & -1 & G_M Z_{in} \\ Z_1 & 0 & 0 & -Z_{in} \\ Z_1 & Z_2 & Z_3 & 0 \end{bmatrix} \begin{bmatrix} I_1 \\ I_2 \\ I_3 \\ I_{in} \end{bmatrix} = \begin{bmatrix} 0 \\ 0 \\ 0 \\ 0 \end{bmatrix} \cdots\cdots (18)$$

$$Z_1 Z_{in} + Z_2 Z_{in} + Z_3 Z_{in} + G_M Z_1 Z_3 Z_{in} + Z_1 Z_2 + Z_1 Z_3 = 0 \cdots\cdots (19)$$

Separating Z_1 and $Z_{\rm ci}$, Eq. (20) defines impedance balance for the oscillation. This relation is valid for the stationary oscillation. Figure 4 shows a single loop circuit of $Z_{\rm cci}$ and the motional impedance.

$$Z_1 + Z_{ci} = 0 \cdots\cdots (20)$$

where,

$$Z_{ci} = \frac{(Z_2+Z_3)Z_{in}}{Z_2+Z_3+(1+G_M Z_3)Z_{in}} = R_{ci} + \frac{1}{j\omega C_{ci}}. \cdots\cdots (21)$$

where $Z_2 = r_{2q} + j\omega L_{2q}$, $Z_3 = \frac{1}{j\omega C_{3o}}$.

The characteristics of the resonator are expressed with the equivalent circuit constant: R_1, L_1, C_1, and C_0. Introducing Z_2, Z_3, $Z_{\rm in}$, and $G_{\rm M}$, $R_{\rm ci}$ and $C_{\rm ci}$ are found. $C_{\rm cx}$ is composed capacitance of $C_{\rm ci}$ and $C_{\rm x}$ in series. Real part of $Z_{\rm ci}$ is $R_{\rm ci}$ is found and the imaginary part is expressed in terms of the reciprocal of equivalent capacitance $C_{\rm ci}$.

$$R_{ci} = \frac{\beta}{\delta}\frac{1+\omega^2\beta\delta\gamma\alpha}{1+(\omega\beta\alpha)^2},$$
$$\frac{1}{C_{ci}} = \frac{\omega^2\beta}{\delta}\frac{\beta\alpha-\delta\gamma}{1+(\omega\beta\alpha)^2}. \cdots\cdots (22)$$

where,

$$\alpha = r_{2q} + R_{in} + \frac{C_m R_{in}}{C_{3o}} - \frac{G_m}{\omega^2 C_{3o} C_{in}},$$
$$\frac{1}{\beta} = \frac{1}{C_{in}} + \frac{1}{C_{3o}}\left(1 + G_m R_{in} + \frac{C_m}{C_{in}}\right) - \omega^2 L_{2q}. \cdots\cdots (23)$$

$$\gamma = r_{2q}R_{in} + \frac{L_{2q}}{C_{in}} - \frac{1}{\omega^2 C_{3o} C_{in}},$$
$$\frac{1}{\delta} = \frac{R_{in}}{C_{3o}} + \frac{r_{2q}}{C_{in}} - \omega^2 L_{2q} R_{in}. \cdots\cdots (24)$$

$$\frac{1}{C_{cx}} = \frac{1}{C_x} + \frac{1}{C_{ci}} \cdots\cdots (25)$$

$R_{\rm cci}$ and $C_{\rm cci}$ are found.

$$R_{cci} = \frac{R_{ci}}{\left(1+\frac{C_0}{C_{cx}}\right)^2 + (\omega C_0 R_{ci})^2},$$
$$\frac{1}{C_{cci}} = \frac{1}{C_0}\left\{1 - \left(1+\frac{C_0}{C_{cx}}\right)\frac{R_{cci}}{R_{ci}}\right\}. \cdots\cdots (26)$$

Here, parallel capacitance C_0 is included in R_{cci} and C_{cci}. Now, the real part of the negative resistance can be compared with R_1 at a glance. The oscillation condition is found in two conditions for stationary oscillation: a comparison of the resistance and the frequency that satisfies the phase matching. Oscillation condition:

$$R_1 + R_{cci} = 0, \cdots\cdots (27)$$

where $R_{cci} < 0$.

Frequency condition:

$$\omega^2 = \frac{1}{L_1}\left(\frac{1}{C_1} + \frac{1}{C_{cci}}\right). \cdots\cdots (28)$$

Apparently, the inequality relation is satisfied in the initial growth of the oscillation.

$$R_1 + R_{cci} < 0 \cdots\cdots (29)$$

The oscillation margin gives the oscillation condition in normalized form:

$$1 \le \frac{|R_{cci}|}{R_1} \cdots\cdots (30)$$

The frequency condition is the basic resonance frequency and the expansion of the oscillation equilibrium due to the negative resistance region. In the stationary oscillation, introducing the resistance condition in the equilibrium, the resonance frequency (28) is recovered.

$$\omega^2 = \frac{1}{L_1}\left(\frac{1}{C_1} + \frac{1}{C_{cci}}\right) - \frac{(R_1+R_{cci})^2}{4L_1^2} \cdots\cdots (31)$$

Apparently, as $R_{\rm cci}$ and $C_{\rm cci}$ are function of ω, a practical method to find the resonance frequency is the conversion of the iteration: the final value is found, when the n-th and n+1-th solutions are equal within a prescribed error.

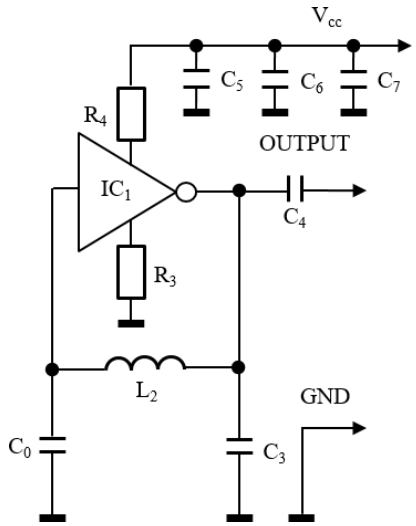

Fig. 5. LC oscillator

$$\omega_{n+1}^2 = \frac{1}{L_1}\left\{\frac{1}{C_1}+\frac{1}{C_{cci}(\omega_n)}\right\}-\frac{\{R_1+R_{cci}(\omega_n)\}^2}{4L_1^2} \cdots\cdots (32)$$

The final value defines the angular oscillation frequency, $\omega_{zt.}$.

$$\omega_{zt} = \omega_n = \omega_{n+1}. \cdots\cdots (33)$$

From the resonance frequency defined by the motion arm f_1, and the difference between ω_{zt} and ω_1 as $\Delta\omega_{zt}$, the frequency deviation normalized by ω_1, $\Delta\omega_{zt}/\omega_1$ is found.

$$\frac{\Delta\omega_{zt}}{\omega_1} = \frac{\Delta f_{zt}}{f_1} \cdots\cdots (34)$$

where $\omega_1 = 2\pi f_1$, $\Delta\omega_{zt} = \omega_{zt} - \omega_1$, $\Delta f_{zt} = f_{zt} - f_1$.

2.2 Analysis of the LC Oscillator Mode As the oscillator circuit includes an inductor in the feedback loop, transition occurs to the LC resonance frequency, when the negative resistance becomes insufficient by the detuning. In this case, the motional impedance disappears and parallel capacitance C_0 is left. Figure 5 shows the circuit diagram of the LC oscillator circuit. The resonator in Fig. 1 is replaced with capacitance C_0. Considering the stray capacitance in inductor L_2 and C_{gd}, simplified LC circuit-1 is found. Applying Kirchhoff's law, the normal equation is found.

$$Z_2 + Z_3 + \frac{(1+G_M Z_3)Z_1 Z_{in}}{Z_1 + Z_{in}} = 0 \cdots\cdots (35)$$

$$Z_{lci} = Z_3 + \frac{(1+G_M Z_3)Z_1 Z_{in}}{Z_1 + Z_{in}} = R_{lci} + \frac{1}{j\omega C_{lci}} \cdots\cdots (36)$$

where

$$Z_1 = \frac{1}{j\omega C_0}. \cdots\cdots (37)$$

The real part of the impedance R_{lci} is found, and the imaginary part of the impedance is expressed in terms of the reciprocal of C_{lci}.

$$R_{lci} = \frac{\beta_l}{\delta_l}\frac{1+\omega^2\beta_l\cdot R_{in}\cdot\delta_l\cdot\gamma_l}{1+(\omega\cdot\beta_l\cdot R_{in})^2},$$
$$\frac{1}{C_{lci}} = \frac{1}{C_{3o}} + \frac{\omega^2\cdot\beta_l}{\delta_l}\frac{\beta_l\cdot R_{in}-\delta_l\cdot\gamma_l}{1+(\omega\cdot\beta_l\cdot R_{in})^2} \cdots\cdots (38)$$

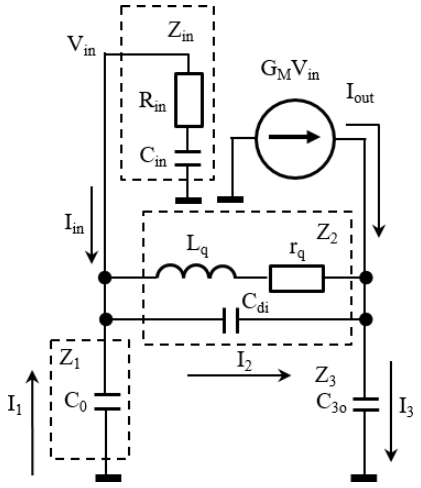

Fig. 6. Simplified LC oscillator circuit: Equivalent LC circuit-1

where

$$\frac{1}{\beta_l} = \frac{1}{C_0} + \frac{1}{C_{in}} \cdots\cdots (39)$$

$$\gamma_l = -\frac{1}{\omega^2 C_{3o}}\left\{\frac{G_m R_{in}}{C_0} - \frac{1}{C_{in}}\left(1+\frac{C_m}{C_{3o}}\right)\right\},$$
$$\frac{1}{\delta_l} = \frac{R_{in}}{C_0}\left(1+\frac{C_m}{C_{3o}}\right) - \frac{G_m}{\omega^2 C_{3o}^2 C_{in}}. \cdots\cdots (40)$$

Figure 6 shows equivalent LC circuit-1. The only difference is that the resonator is replaced by parallel capacitance C_0. Following equivalent circuit-2 and equivalent circuit-3, the oscillator circuit is simplified to a single loop circuit. C_{di} is composed with Z_{lci}. Equivalent impedance Z_{lcci} is found. The real part is resistance R_{lcci}. The imaginary part is positively polarized and expressed in terms of the reciprocal of C_{lcci}.

$$R_{lcci} = \frac{R_{lci}}{\left(1+\frac{C_{di}}{C_{lci}}\right)^2 + (\omega C_{di} R_{lci})^2},$$
$$\frac{1}{C_{lcci}} = \frac{1}{C_{di}}\left\{1-\left(1+\frac{C_{di}}{C_{lci}}\right)\frac{R_{lcci}}{R_{lci}}\right\}. \cdots\cdots (41)$$

From the phase matching condition, the angular frequency of the LC oscillation ω_{lc} is found.

$$\omega_{lc}^2 = \frac{1}{L_q C_{lcci}}. \cdots\cdots (42)$$

where $\omega_{lc} = 2\pi f_{lc}$.

$$r_q + R_{lcci} \le 0, \cdots\cdots (43)$$

For the stationary oscillation: $r_p + R_{lcci} = 0$.

Oscillation condition is given as the normalized negative resistance equal to or larger than unity.

Oscillation condition:

$$1 \le \frac{|R_{lcci}|}{r_q} \cdots\cdots (44)$$

Frequency condition:

$$\omega^2 = \frac{1}{L_q C_{lcci}} - \frac{(r_q + R_{lcci})^2}{4L_q^2} \cdots\cdots (45)$$

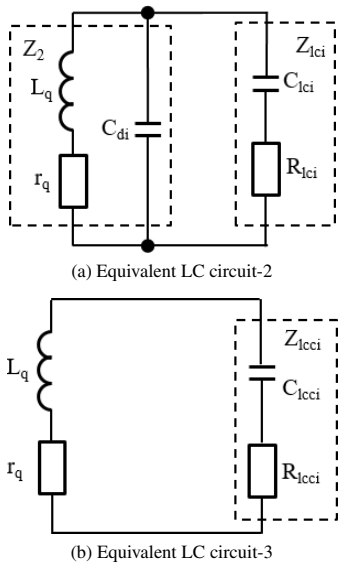

(a) Equivalent LC circuit-2

(b) Equivalent LC circuit-3

Fig. 7. Simplified LC oscillator circuit

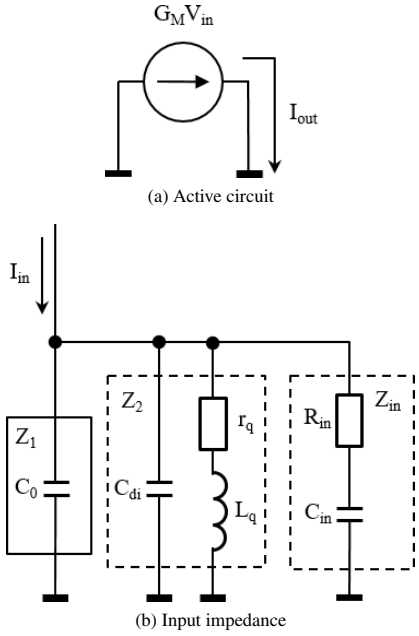

(a) Active circuit

(b) Input impedance

Fig. 8. Equivalent circuit for the f_T model of CMOS inverter

As R_{lcci} and C_{lcci} depend on ω, the oscillation frequency is determined by the convergence of the series of solutions.

$$\omega_{n+1}^2 = \frac{1}{L_q C_{lcci}(\omega_n)} - \frac{\{r_q + R_{lcci}(\omega_n)\}^2}{4L_q^2} \cdots\cdots (46)$$

where $\omega_{lc} = 2\pi f_{lc}$, $\omega_{lc} = \omega_{n+1} = \omega_n$.

2.3 Oscillation Frequency Limit Transition frequency f_{T} defines a measure for high-frequency gain of active devices. It is defined as the frequency that, at the small signal gain, the ratio of output current and input current become unity. This factor is strongly influenced by the capacitance between the input-output terminals and between the input-terminal and ground. In case of the MOSFET, this transition frequency is found [8].

$$f_T = \frac{g_m}{2\pi(c_{gd} + c_{gs})} \cdots\cdots (47)$$

where $C_{\mathrm{p:gd}}$ and $C_{\mathrm{p:gs}}$, $C_{\mathrm{n:gd}}$ and $C_{\mathrm{n:gs}}$ are pairs of gate-drain and gate-source capacitances. The frequency characteristics are also influenced by stray capacitance c_{os} and c_{io}. Figure 8 shows an equivalent circuit of a CMOS inverter. While motion arm current is not excited, the resonator shows only capacitance C_0. The transition frequency f_{T}-model is found for the unity gain. Then, the parallel impedance of Z_1, Z_2, and Z_{in} are reduced to admittance Y_{T}, conductance G_{T}, and capacitance C_{T}. The f_{T}-model-2 is found. When capacitance C_{T} is negatively polarized, the reactance is converted to inductance L_{T}.

The impedance is composed to single admittance and reactance.

$$Y_T = \frac{1}{Z_1} + \frac{1}{Z_2} + \frac{1}{Z_{in}} = G_T + j\omega C_T. \cdots\cdots (48)$$

$$L_T = -\frac{1}{\omega^2 C_T}. \cdots\cdots (49)$$

$$\frac{1}{Z_2} = j\omega C_{di} + \frac{1}{r_q + j\omega L_q}. \cdots\cdots (50)$$

Setting the input voltage, the output and input current ratio is found.

$$\frac{I_{out}}{I_{in}} = \frac{G_M}{Y_T} = \frac{G_m + j\omega C_m}{G_T + j\omega C_T}. \cdots\cdots (51)$$

where $I_{in} = Y_T V_{in}$, $I_{out} = G_M V_{in}$.

The absolute value of the current gain is found. F_{T} is defined as the frequency where the current gain is reduced to unity.

$$\left|\frac{I_{out}}{I_{in}}\right| = \frac{\sqrt{(G_m G_T + \omega^2 C_m C_T)^2 + \omega^2 (C_m G_T - C_T G_m)^2}}{G_T^2 + (\omega C_T)^2} \cdots\cdots (52)$$

3. Experimental Result and Discussions

Figure 9 shows the frequency dependence of oscillation margins $|R_{\mathrm{cci}}|/R_1$ and $|R_{\mathrm{lcci}}|/r_{\mathrm{p}}$ for different values of transconductance g_{m}.

The oscillation margin shows a wider frequency region and a lower peak when g_{m} is increased. In the case of Lamb wave and SAW resonator, $|R_{\mathrm{cci}}|/R_1$ is larger than unity from 430 MHz to 448 MHz, for $g_{\mathrm{m}} = 0.4$ mA/V, and shows its maximum value of 58 at 439 MHz. For $g_{\mathrm{m}} = 0.5$ mA/V, $|R_{\mathrm{cci}}|/R_1$ is larger than unity from 420 MHz to 448 MHz, and shows its maximum value of 14 at 430 MHz. For $g_{\mathrm{m}} = 0.6$ mA/V, $|R_{\mathrm{cci}}|/R_1$ is larger than unity from 413 MHz to 444 MHz, and shows its maximum value of 5 at 423 MHz. In the case of LC oscillation, $|R_{\mathrm{lcci}}|/r_{\mathrm{p}}$ is larger than unity at $g_{\mathrm{m}} = 0.4$ mA/V at frequencies lower than 405 MHz. The oscillation limit is higher for increased values of g_{m}. For example, the oscillation limit 452 MHz for $g_{\mathrm{m}} = 0.5$ mA/V and 493 MHz for $g_{\mathrm{m}} = 0.6$ mA/V. No oscillation condition meets for g_{m} smaller than 0.38 mA/V at frequency higher than 400 MHz.

Figure 10 shows oscillation margin $|R_{\mathrm{cci}}|/R_1$ and $|R_{\mathrm{lcci}}|/r_{\mathrm{q}}$, the oscillation frequency of the resonance oscillation f_{zt}, normalized frequency shift $\Delta f_{\mathrm{zt}}/f_1$ and the oscillation frequency

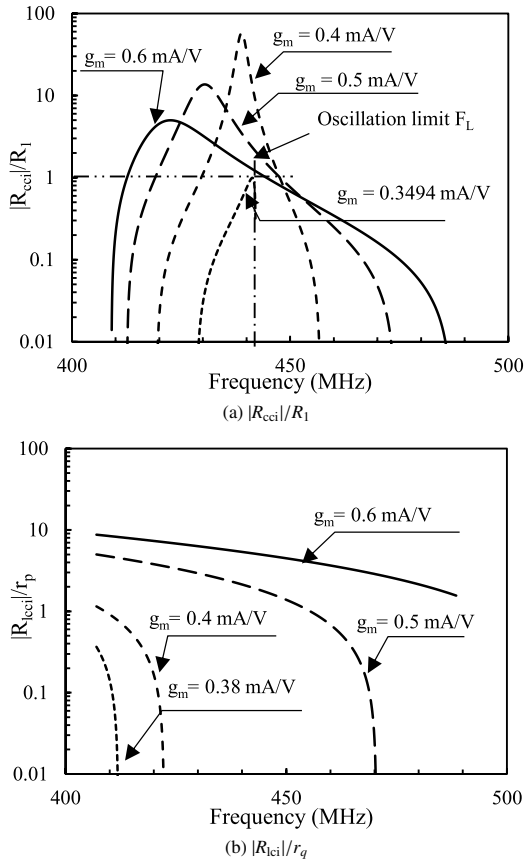

Fig. 9. Comparison of oscillation margins $|R_{cci}|/R_1$ and $|R_{lci}|/r_q$ as functions of frequency. Circuit constant: L_2 = 47 nH; r_P = 1.44 Ω; c_p = 0.37 pF; c_{io} = 0.1 pF; c_{gd} = 0.01 pF; c_{di} = 0.12 pF; R_f = 47 Ω; C_{gs} = 1.5 pF; c_0 = 2.8 pF; C_x = 1000 pF. Equivalent circuit constant of the resonator: C_0 = 4.1 pF; R_1 = 22.9 Ω

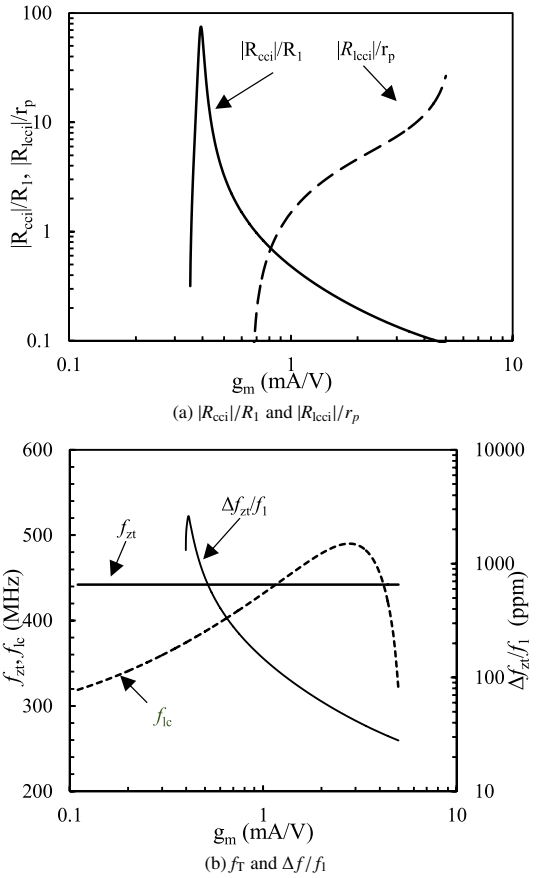

Fig. 10. Oscillation margin $|R_{cci}|/R_1$, $|R_{lci}|/r_q$, oscillation frequencies f_{osc}, f_{lc}, and normalized frequency deviation $\Delta f_{zt}/f_1$ as functions of g_m. Circuit constant: L_2 = 47 nH; r_P = 1.44 Ω; c_p = 0.37 pF; c_{io} = 0.1 pF; c_{gd} = 0.01 pF; c_{di} = 0.12 pF; R_f = 47 Ω; C_{gs} = 1.5 pF; c_0 = 2.8 pF; C_x = 1000 pF. Equivalent circuit constant of the resonator: C_0 = 4.1 pF; R_1 = 22.9 Ω

of the LC oscillation f_{lc} as functions of g_m. Oscillation margin $|R_{cci}|/R_1$ exceeds unity and oscillation condition of the resonance oscillation is fulfilled for g_m from 0.36 mA/V to 0.65 mA/V and shows its maximum at 0.4 mA/V.

The maximum value of oscillation margin $|R_{cci}|/R_{1:max}$ is approximately 75. Oscillation margin $|R_{lcci}|/r_q$ exceeds unity for g_m larger than 0.9 mA/V and the oscillation condition of the LC oscillation is fulfilled.

In summary, g_m in the initial growth of the resonance oscillation is 0.7 mA/V, then after the maximum growth at 0.4 mA/V and decreases to 0.35 mA/V in the stationary oscillation. In a good contrast, the LC oscillation occurs at the frequency where the largest g_m is obtained at the initial growth. The oscillation condition of the negative resistance of the LC oscillation becomes insufficient when the transconductance deceases to 0.9 mA/V, where in our scenario a transition occurs to crystal resonance oscillation.

In crystal resonance, higher negative resistance is generated at smaller g_m. The oscillation frequency is approximately constant at 442 MHz, and the normalized frequency deviation is 453 ppm at g_m = 0.4 mA/V, and 330 ppm at g_m = 0.65 mA/V. The oscillation frequency in the stationary oscillation is obtained at smaller g_m of the resonance oscillation. The oscillation of LC resonance tends to be the frequency where the highest g_m can be obtained at the initial growth. At g_m = 2.8 mA/V, the oscillation frequency is

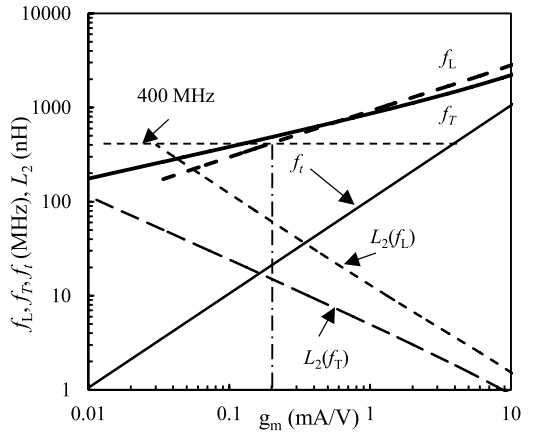

Fig. 11. f_L, f_T, f_t, and necessary L_2 as functions of g_m. Circuit constants: L_2 variable parameter; r_P = 0.0001 Ω; c_p = 0.0001 pF; c_{io} = 0.1 pF; c_{gd} = 0.01 pF; c_{di} = 0.12 pF; R_f = 47 Ω; C_{gs} = 1.5 pF; c_0 = 2.8 pF; C_x = 1000 pF; C_0 = 4.1 pF; R_1 = 22.9 Ω

initially 490 MHz. Then, along with the decrease in g_m and the growth of oscillation amplitude, at g_m = 0.9 mA/V, the oscillation frequency decrease to approximately 424 MHz.

Figure 11 shows the g_m dependence of the lower limit of the oscillation, where F_T in (51) is the limit frequency at

Table 4. Transition frequency F_T and oscillation limit F_L

g_m (mA/V)	F_T (GHz)	L_2 (nH)
0.11	0.4	22
1	0.9	5
4	1.5	1.9
g_m (mA/V)	F_L (GHz)	L_2 (nH)
0.1	0.3	110
0.65	0.4	60
1	0.9	11
4	1.8	3.7

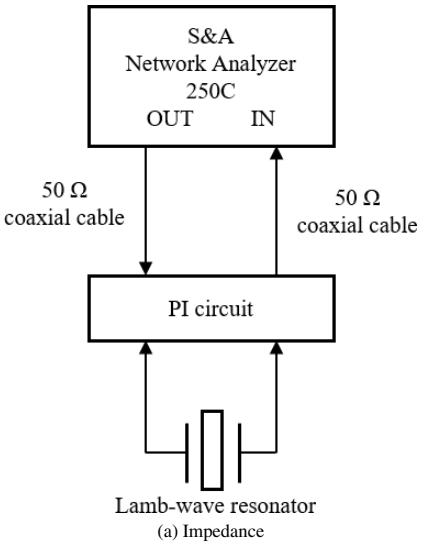

(a) Impedance

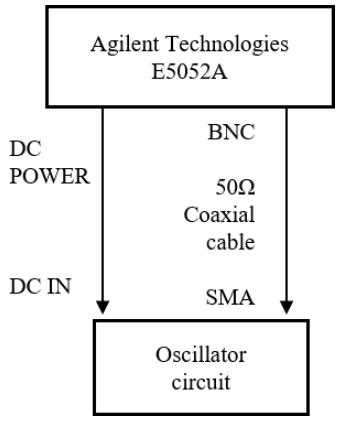

(b) Phase-noise characteristics

Fig. 12. Experimental setup for measurement of impedance and the phase noise characteristics

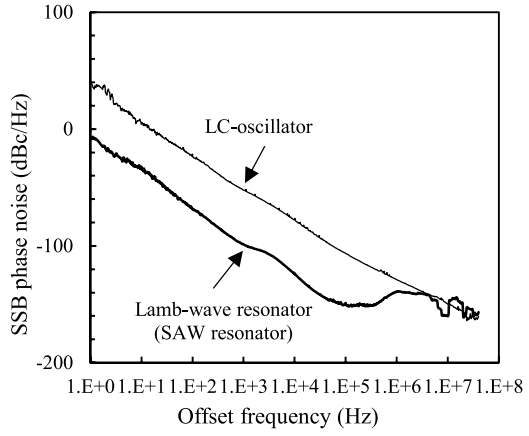

(a) SSB phase noise

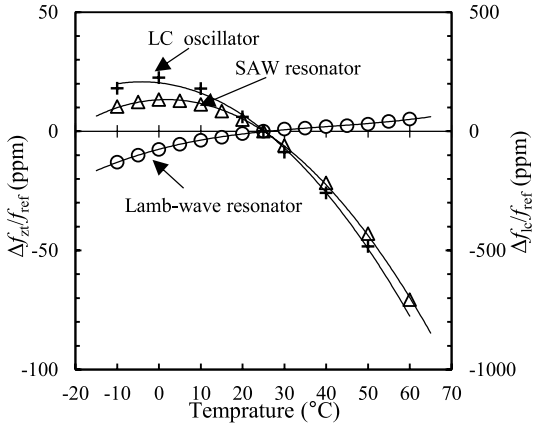

(b) $\Delta f_{zt}/f_{ref}$ and $\Delta f_{lc}/f_{ref}$

Fig. 13. Experimental comparison of SSB phase noise and the oscillation frequency. Reference f_{ref} is measured at 25°C. In the case of LC oscillation, the resonator is replaced with a capacitor, 2 pF

$|I_{out}/I_{in}|$ equal to unity and F_L in (30) is the limit frequency at $|R_{cci}|/R_1$ equal to unity, compared with the transition frequency of the CMOS inverter in (46) L_2 is an ideal inductance. f_t increases proportionally. Apparently indicating f_t = 400 MHz at g_m = 4 mA/V. Transconductance larger than 4 mA/V is necessary for the operation at the 400 MHz range.

Apparently, F_T and F_L are approximately equal values at the same g_m, and this characteristics is apparent at the high frequency side. F_T and F_L are higher than the characteristic values of f_t. Although F_T and F_L show approximately equal values at the same g_m, the required values of L_2 are different. For example, the value necessary is 22 nH for F_T = 400 MHz, but 60 nH is necessary for F_L = 400 MHz. Logically, in the test circuit for F_L, larger inductance is necessary for the establishment of the same resonance frequency because the capacitance C_{3o} is connected in series to the internal capacitor. As the intersection of f_t with 400 MHz is 4 mA/V, it is necessary that g_m is greater than 4 mA/V to establish the stationary oscillation. The effect of the insertion of inductance L_2 reduces the necessary value of g_m to 0.1 mA/V, at the intersection of F_T with 400 MHz. Similarly, the necessary value of g_m is reduced to 0.2 mA/V, at the intersection of F_L with 400 MHz. This result suggests that the oscillation condition for the stationary crystal resonance oscillation is fulfilled at smaller values of g_m by the insertion of appropriate inductance. Table 4 summarizes the necessary value of L_2 to realize the stationary oscillation.

Figure 12 shows an experimental setup for comparison of the SSB phase noise of the Lamb-wave resonator oscillator.

Experimental facilities consists of a 250C Network Analyzer, a high speed-computer controlled network analyzer (Saunders and Associates, Phoenix, AZ, USA) with temperature-controlled mount, and an Agilent E5052A, Signal Source Analyzer, (Agilent Technologies, Santa Clara, CA, USA). Figure 13 shows an experimental comparison of the phase noise and the dependence of the frequency deviation on the ambient temperature.

Discussion on the stability of time-base is based on two

Table 5. Normalized frequency deviation

Resonator	Minimum (ppm)	Maximum (ppm)	Span (ppm)
Lamb-wave	-13 (-10°C)	5 (60°C)	18
SAW	-71 (60°C)	13 (0°C)	84
LC oscillator	-483 (50°C)	225 (0°C)	708

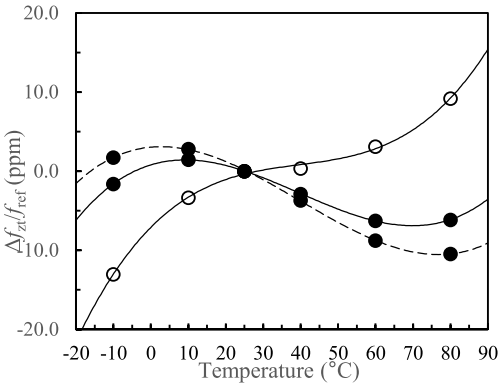

Fig. 14. Temperature dependence of the oscillation frequency of the Lamb-wave resonator oscillator. Reference f_{ref} is measured at 25°C

methods: the 2-sample standard deviation in the time domain and the SSB-phase noise in the frequency domain. In this work, the SSB phase noise shows flat characteristics at −150 dBc/Hz at frequencies over 100 kHz, and dependence of −10 dB per decade, at frequencies lower than 100 kHz. No significant difference can be observed between the SAW and Lamb-wave resonators. The LC oscillation shows 10 dBc/Hz lower values at frequencies lower than 100 kHz.

The SAW resonator oscillator shows a square temperature dependence, and the Lamb-wave resonator oscillator shows cubic dependence similar to an AT-cut crystal resonators. Lamb wave resonator shows better stability compared with the SAW resonator. The maximum deviation of each resonators is compared in Table 5.

Figure 14 shows typical examples of the temperature dependence of the oscillation frequency, where the interpolation is calculated with third order polynomial functions. The Lamb wave mode shows a thickness-shear vibration as well as motion perpendicular to the surface. Because the slab thickness is approximately one wave length, the oscillation mode is influenced by many production factors, the cut angle, scatter in the thickness of the crystal and the electrode pattern. The characteristics, otherwise stated, can be controlled by these process parameters to reduce the temperature dependence.

4. Conclusion

In this work, we proposed a design of the oscillator circuit for the Lamb wave resonator at 442 MHz, using a low cost general purpose single-gate CMOS-Inverter. The primary idea is the compensation of the internal capacitance using an inductor connected between the input and the output terminals. This scheme is simple at a glance, but the oscillator circuit works on a complicated principle that was explained and demonstrated in the experiment.

The first engineering issue in this work is the separation of the LC oscillation. The transconductance in the crystal resonance oscillation varies in the startup of the stationary oscillation. In our scenario, the transconductance of the CMOS inverter is controlled by the feedback resistor so that g_m is sufficiently large at the initial stage of small signal gain, and reduced to balance with the dissipation in the stationary oscillation. The oscillation condition for the crystal resonance oscillation is fulfilled for $0.36\,\mathrm{mA/V} < g_m < 0.65\,\mathrm{mA/V}$. In a good contrast, the oscillation condition for the LC oscillation is fulfilled for $0.9\,\mathrm{mA/V} < g_m$. From the analysis of the oscillation limit, we can say that the operational frequency region can be expanded by the resonance pole generated by the insertion of the appropriate inductance. By the inductive enhancement of the negative resistance, the necessary transconductance for F_T can be realized at $g_m > 0.1\,\mathrm{mA/V}$. Similarly, the oscillation limit $F_L > 400\,\mathrm{MHz}$ is realized at $g_m > 0.2\,\mathrm{mA/V}$. SSB phase noise characteristics shows −150 dBc/Hz at offset frequency higher than 100 kHz, and satisfies the industrial requirement for the stability of quartz crystal resonator. The temperature drift of the proposed oscillator circuit with the Lamb-wave resonator shows high temperature stability compared with the SAW resonator.

References

(1) J. Matsuoka, T. Sato, and T. Ohshima: “A Circuit for High-Frequency Crystal Oscillators”, Proceedings of the IEEE International Frequency Control Symposium, pp.569–74 (2003)

(2) B. Razavi: “Design of Analog CMOS Integrated Circuits”, McGraw-Hill Companies (2001)

(3) Y. Nakagawa, S. Tanaka, and S. Kakio: “Lamb-Wave-Type High Frequency Resonator”, Japanese Journal of Applied Physics, Vol.42, No.1, pp.3086–3090 (2003) doi:10.1143/JJAP.42.3086

(4) Y. Nakagawa, M. Momose, and S. Kakio: “Characteristics of Reflection of Resonators Using Lamb Wave on AT-Cut Quartz”, Japanese Journal of Applied Physics, Vol.43, No.5B, pp.3020–3023 (2004) doi:10.1143/JJAP.43.3020

(5) Y. Nakagawa, M. Shigeda, and S. Kakio: “Temperature Characteristics of Substrates for Lamb-Wave-Type Acoustic Wave Devices”, Japanese Journal of Applied Physics, Vol.45, No.1, pp.4667–4670 (2006) doi:10.1143/JJAP.45.4667

(6) Y. Nakagawa, M. Momose, and S. Kakio: “Resonators Using a Lamb Wave on AT-Cut Quartz”, Proceedings of Symposium Ultrasonic Electronics, Vol.27, pp.79–80 (2006)

(7) Y. Nakagawa, M. Momose, and S. Kakio: “Resonators Using a Lamb Wave on AT-Cut Quartz”, Japanese Journal on Applied Physics, Vol.46, p.4665 (2007) doi:10.1143/ JJAP.46.4665

(8) H. Yoshida, Y. Nakagawa, and S. Kakio: “Propagation Characteristics of Substrate for Lamb-Wave-Type Elastic Wave Devices”, Japanese Journal on Applied Physics, Vol.48, Special Issue: Ultrasonic Electronics, 07GF02, pp.1–3 (2009) doi:10.1143/ JJAP.48.07GF02

(9) P.R. Gray, P. Hurst, S. Lewis, and R.G. Meyer: “Analysis and Design of Analog Integrated Circuits”, 5th ed., Wiley, New York, p.67 (2001)

Tomio Sato (Non-member) graduated from the Department of Electronics, Yamanashi University, in March 1971. Engaged in the development of high-stability quartz crystal oscillators at Toyo-Communication Equipment Co. Ltd. He holds a degrees of Doctor of Medicine and Engineering from the University of Yamanashi. Presently, he is in charge as a lecturer at the University of Yamanashi.

Masahide Marumo (Non-member) graduated from the Department of Electrical Engineering, University of Yamanashi, in March 1985. Presently, he is in charge as the General Manager, River Eletec Corp. Ltd. Inc. Nirasaki-city, Yamanashi-Prefecture, Japan.

Tetsuya Akitsu (Member) graduated from the Department of Electronics, Kyoto University, in March 1974. He holds degrees of Master and Doctor of Engineering from Kyoto University. Presently, he is a professor in the Integrated Graduate School of Medicine, Engineering, and Agricultural Science, University of Yamanashi.